J MATER RES TECHNOL. 2019;8(1):1550–1565

Available online at www.sciencedirect.com

jmr&t Journal of Materials Research and Technology

www.jmrt.com.br

Review Article

Dislocation Burgers vector and the Peach–Koehler force: a review

Vlado A. Lubarda

Department of NanoEngineering, University of California, San Diego, La Jolla, CA 92093-0448, USA

ARTICLE INFO

Article history:
Received 10 May 2018
Accepted 20 August 2018
Available online 10 December 2018

Keywords:
Burgers circuit
Burgers vector
Climb force
Dislocation loop
Glide force
Image stress
J integral
Osmotic force
Peach–Koehler force
Potential energy
Virtual work

ABSTRACT

Different definitions of the Burgers vector and the corresponding construction of the Burgers circuit for dislocation loops and straight dislocations, created by the displacement discontinuity imposed across different surface cuts are reviewed. This is used as a geometric background for the derivation and discussion of the Peach–Koehler expression for the energetic force exerted on a dislocation by different sources of stress. Three approaches were used and compared: (i) the classical virtual work approach of Peach and Koehler, extended to include the changes in size and shape of the dislocation loop; (ii) the potential energy approach which allows the incorporation of the effects of image stresses; and (iii) the approach based on the evaluation of the *J*-integral. The glide and climb components of the dislocation force are determined and discussed for continuum and lattice dislocations.

Vlado A. Lubarda received his mechanical Dipl. Eng. degree from the University of Montenegro in 1975, and his M.S. and Ph.D. degrees from Stanford University in 1977 and 1979. He was an Assistant and Associate Professor at the University of Montenegro from 1980-1989, Fulbright Fellow and Visiting Associate Professor at Brown University from 1989 to 1991, and the Arizona State University from 1992 to 1997. Since 1998, he is an Adjunct Professor of Applied Mechanics in the Department of Mechanical and Aerospace Engineering of the University of California, San Diego. He is also a Research Affiliate of CMRR and since 2013 a Distinguished Teaching Professor in the UCSD's NanoEngineering Department. Dr. Lubarda has done research work in the fields of elasticity, plasticity, viscoelasticity, dislocation theory, damage mechanics, nano and biomechanics. He is the author of numerous journal and conference publications, and four books: *Strength of Materials* (University of Montenegro Press, 1985), *Elastoplasticity Theory* (CRC Press, 2002), *Mechanics of Solids and Materials* (Cambridge University Press, 2006), and *Topics in Solid Mechanics: Elasticity, Plasticity, Damage, Nano and Biomechanics* (Obod Press, 2013). Dr. Lubarda serves on the editorial board of *Theoretical and Applied Mechanics*, *Mathematics and Mechanics of Solids*, and *Acta Mechanica*. Professor Lubarda is the recipient of the Barbara and Paul Saltman Distinguished Teaching Award, four Teacher of the Year Awards in the MAE and NanoEngineering Departments, and three Tau Beta Pi Outstanding Teacher of the Year Awards for Engineering. He is also a Fellow of Revelle College, the oldest of the six UCSD colleges. Dr. Lubarda is a member of the Montenegrin Academy of

E-mail: vlubarda@ucsd.edu

https://doi.org/10.1016/j.jmrt.2018.08.014

Sciences and Arts, the Montenegrin Academy of Engineering, and the European Academy of Sciences and Arts.

1. Introduction

Dislocation mechanics is a formidable discipline that has enabled engineers to understand, predict, and control the mechanical response of metals and ceramics in the plastic range of their deformation. It has import in ductility, hardening and strengthening mechanisms, fracture, fatigue, creep, and a broad range of other phenomena. A rigorous field of endeavor, it traces its roots to three seminal papers published in 1934 by Orowan [1], Polanyi [2], and Taylor [3]. The foundations of dislocation mechanics, with early contributions by Volterra in 1907 [4], and the entire construct are based on elasticity theory, which provides the background stresses and strains upon which the dislocations (and twins, phase boundaries) move. The quantitative treatment of dislocations and the development of the physical theory of plasticity would not have been possible if it were not for two equations, which link continuum and dislocation theory: (a) the Orowan equation which relates the rate of macroscopic shear strain to the density of dislocations and the average dislocation velocity; and (b) the Peach–Koehler equation, which relates the stress field in the material to an effective (energetic) force acting on a dislocation. This review is devoted to the latter equation.

The energetic, also referred to as a configurational force acting on a dislocation loop plays a fundamental role in continuum mechanics and materials science studies of dislocations, their motion and interactions among themselves or with other defects, such as inclusions, free surfaces, and interfaces. The expression for this force (per unit length of a dislocation loop) was first derived in the form $\mathbf{f}=(\boldsymbol{\sigma}\cdot\mathbf{b})\times\boldsymbol{\xi}$ by Peach and Koehler [5]. The stress state $\boldsymbol{\sigma}$ at the considered point of the dislocation loop is caused by applied loading or interaction of the dislocation with other dislocations or defects, but excludes the self-stress from the dislocation itself. The Burgers vector of the dislocation $\mathbf{b}$ represents the displacement discontinuity imposed to create the dislocation, while $\boldsymbol{\xi}$ is the unit vector tangential to the dislocation loop at the considered point (Fig. 1). We use boldface symbols for vectors and tensors throughout; for most of the text, we adopt the direct tensor notation, rather than the indicial notation.

For example, for an infinitely long edge dislocation along the z-direction, with the Burgers vector $\mathbf{b}=b_x\mathbf{e}_x$ and with the positive direction of the dislocation line vector out of the plane of figure ($\boldsymbol{\xi}=\mathbf{e}_z$), the dislocation force is $\mathbf{f}=\sigma_{xy}b_x\mathbf{e}_x-\sigma_{xx}b_x\mathbf{e}_y$, where σ_{xy} and σ_{xx} are the shear and normal stresses at the location of the dislocation, excluding the singular stresses from the dislocation itself. In this expression, the glide component of the dislocation force is $\mathbf{f}_{\text{glide}}=\sigma_{xy}b_x\mathbf{e}_x$, while $\mathbf{f}_{\text{climb}}=-\sigma_{xx}b_x\mathbf{e}_y$ is the climb component. If the positive direction of the dislocation line vector is taken to be into the plane of figure ($\boldsymbol{\xi}=-\mathbf{e}_z$), the same edge dislocation is characterized by the Burgers vector $\bar{\mathbf{b}}=-\mathbf{b}$, which is opposite to the Burgers vector of the previously considered dislocation with the line vector $\boldsymbol{\xi}=\mathbf{e}_z$. In this case, the Peach–Koehler expression gives for the dislocation force $\mathbf{f}=-\sigma_{xy}\bar{b}_x\mathbf{e}_x+\sigma_{xx}\bar{b}_x\mathbf{e}_y$, so that the glide and climb components are $\mathbf{f}_{\text{glide}}=-\sigma_{xy}\bar{b}_x\mathbf{e}_x$ and $\mathbf{f}_{\text{climb}}=\sigma_{xx}\bar{b}_x\mathbf{e}_y$. Since $\bar{b}_x=-b_x$, the same dislocation forces, in magnitude and direction, are obtained as in the previous case. In some studies and textbooks on dislocations (e.g., [6–10]), one direction of the dislocation line vector is taken as positive, while in others (e.g., [11,12]), the opposite direction is taken as positive. Although both directions are permissible choices, a care is needed to properly identify the corresponding direction of the Burgers vector of the dislocation, and avoid the sign errors in the derivation of the expression for the dislocation force, first pointed out by de Wit [13] and further discussed by Hirth and Lothe [8].

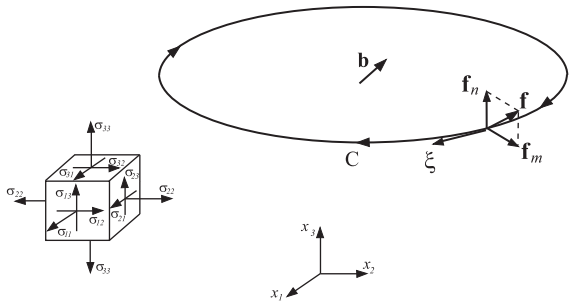

Fig. 1 – A plane dislocation loop C with a Burgers vector b in a medium under the stress field σ. The unit vector tangential to the loop at a considered point is ξ. The component of the dislocation force f orthogonal to the plane of the loop is $\mathbf{f}_n$ and within the plane of the loop is $\mathbf{f}_m$. Both components are orthogonal to C.

The purpose of this review is to shed additional light to this topic which is of significance for the derivation of the Peach–Koehler expression for the energetic force acting on a dislocation loop. In Section 2, we review different definitions of the Burgers vector used in the literature and the corresponding construction of the Burgers circuit for dislocation loops created by the displacement discontinuity imposed across different surface cuts. With this as a geometric background, we derive in Section 3 the Peach–Koehler expression for the force on a dislocation loop in an infinite medium, caused by mechanical stress excluding the self-stress from the dislocation itself. This is accomplished by the virtual work consideration, as in Peach and Koehler [5], except that a virtual change of the dislocation configuration is not restricted to be of a translational type, but may also include a size and shape change of the loop. The glide and climb components of the dislocation force are derived for an arbitrary loop, and in particular for circular glide and circular sessile dislocation loops. We also discuss the osmotic or chemical force on a lattice dislocation. In Section 4 we generalize the derivation from Section 3 by including in the analysis the contribution from the image stresses of the dislocation, associated with the boundary of a finite body in which the dislocation resides. This is done by the consideration of the potential energy. The elastic field represented as the sum of the elastic field of the dislocation embedded in an infinite medium, and the image field. The final expression for the dislocation force is $\mathbf{f}=[(\boldsymbol{\sigma}+\hat{\boldsymbol{\sigma}}+\boldsymbol{\sigma}^{\text{int}})\cdot\mathbf{b})]\times\boldsymbol{\xi}$, where $\hat{\boldsymbol{\sigma}}$ is the image stress from all dislocations, including the dislocation under consideration, and $\boldsymbol{\sigma}^{\text{int}}$ is the stress due to interaction of the dislocation with

other dislocations or other defects, if present in the body. Section 5 is devoted to the derivation of the Peach–Koehler force on an infinitely long straight dislocation in a finite body under plane strain conditions by the evaluation of the *J*-integral.

2. Direction of the Burgers vector

It is well-known (e.g., [8,14,9,15]) that, for a given displacement discontinuity across the 'cut surface' used to create a dislocation, the Burgers vector of the dislocation can be defined to have either of the two senses of the direction of the relative displacement between the two surfaces of the cut. This can be illustrated in various ways; we conveniently choose the case of an edge dislocation created by relative displacement between the cut surfaces along the positive *x*-axis (Fig. 2). In Fig. 2a, the lower surface of the cut is displaced relative to the upper surface by the amount *b* to the right, while in Fig. 2b the upper surface of the cut is displaced relative to the lower surface by the amount *b* to the left. Shown are the corresponding Burgers circuits emanating from the starting point *S* to the finishing point *F*. If the Burgers vector is defined as the vector connecting the points *S* and *F*, from *S* to *F*, i.e., $\mathbf{b} = \mathbf{SF}$, then, for the case shown in Fig. 1a,

$$\oint_C \mathrm{d}\mathbf{u} = \mathbf{b}\,, \quad \oint_C \mathrm{d}u_x = b \tag{2.1}$$

while, for the case shown in Fig. 2b,

$$\oint_C \mathrm{d}\mathbf{u} = \mathbf{b}\,, \quad \oint_C \mathrm{d}u_x = -b \tag{2.2}$$

The two so-defined Burgers vectors are clearly opposite, though the stress and strain fields are the same in both cases. The corresponding displacement fields differ by a rigid-body translation, such that $u_x^{(a)} = u_x^{(b)} + b$. Note that in (2.1) the Burgers circuit is counterclockwise, while in (2.2) it is clockwise (relative to an observer at positive *z*).

Since the Burgers circuit in Fig. 2a is counter-clockwise, the unit vector of the dislocation line $\boldsymbol{\xi}$ is taken to be in the positive *z*-direction ($\boldsymbol{\xi} = \mathbf{e}_z$), while for the clockwise Burgers circuit in Fig. 2b the unit vector of the dislocation line is taken to be in the negative *z*-direction ($\boldsymbol{\xi} = -\mathbf{e}_z$). With this choice of the direction for $\boldsymbol{\xi}$, the integrals in (2.1) and (2.2) are both taken in a right-handed sense relative to $\boldsymbol{\xi}$. Furthermore, in each case, the first crossed surface of the cut, in the immediate passing from one surface of the cut to the other, is the surface which moves by $\mathbf{b}$ relative to the other surface of the cut. Denoting these two surfaces by Σ_1 and Σ_2, we can write $\mathbf{b} = \mathbf{u}_1 - \mathbf{u}_2$ for any two points originally coincident on the surface along which the cut is made. The Burgers vector in either case can be referred as being based on the RH/SF (right-handed, start-to-finish) convention. In the first case (Fig. 2a), the sliding surface Σ_1 is below the cut ($y = 0, x > 0$), and in the second case (Fig. 2b) it is above that cut. In the context of crystalline dislocations, the extra half-plane of atoms for an edge dislocation is found by

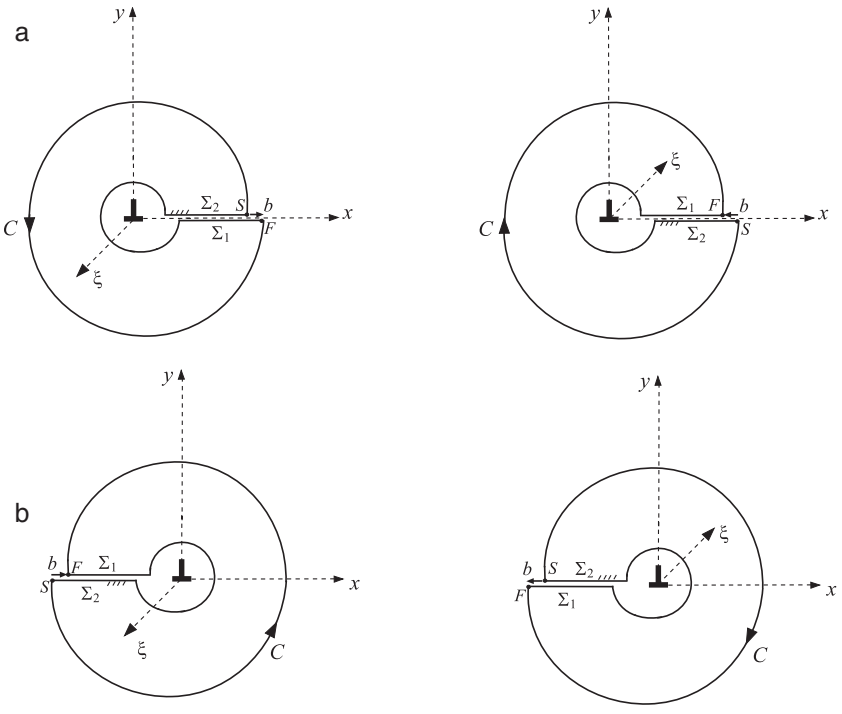

Fig. 2 – An edge dislocation created by the displacement discontinuity *b* along the positive *x*-axis. In part (a) the lower surface Σ_1 of the cut is displaced by *b* to the right, while the upper surface Σ_2 is fixed; (b) the upper surface Σ_1 is displaced by *b* to the left, while the lower surface Σ_2 is fixed; parts (c) and (d) are the same as parts (a) and (b), except that the displacement discontinuity is imposed along the negative *x*-axis. In each case, indicated are the corresponding directions of the dislocation line vector ξ (orthogonal to the plane of figure), and the direction of the Burgers circuit, which is right-handed with respect to ξ. The Burgers circle begins at the point *S* and ends at the point *F*, so that the Burgers vector is $\mathbf{b} = \mathbf{SF}$.

making a 90° rotation of the Burgers vector in a right-handed sense with respect to $\boldsymbol{\xi}$. If the screw dislocation component is added, the right-handed screw dislocation is created by the displacement of Σ_1 in the positive $\boldsymbol{\xi}$ direction.

If the displacement discontinuity is imposed across the cut made along the negative x-axis, the Burgers circuits are as shown in Fig. 2c and d. The corresponding Burgers vectors are specified by the RH/SF convention, with the indicated sliding surface Σ_1 in each case. The Burgers vector definition used in Fig. 2b and d has been adopted by Hirth and Lothe [8, p. 23], and [16, p. 122], among others. It is also equivalent to the RH/SF convention used by de Wit [13], according to which **b** points to the right when an observer looks along $\boldsymbol{\xi}$ for an edge dislocation with the extra half plane below the glide plane (and thus to the left for an edge dislocation with the extra half plane above the glide plane, as in Fig. 2b and d). See also a discussion by Teodosiu [17, p. 101].

The described information about the created dislocation needs to be specified in order to correctly derive the Peach–Koehler force on the dislocation, considered in Section 3 of this paper. For example, if $\boldsymbol{\nu}$ is the unit vector orthogonal to Σ_1, directed towards Σ_2, the specific work (per unit area of the cut surface) done by the externally induced traction $\mathbf{t}_\nu$ on the displacement discontinuity **b** is $\mathbf{t}_\nu \cdot \mathbf{b}$. For the edge dislocation in Fig. 2a, this is $\mathbf{t}_y \cdot \mathbf{b}$, while for the edge dislocation in Fig. 2b, it is $\mathbf{t}_{-y} \cdot \mathbf{b}$. Since the Burgers vectors in Fig. 2a and b are opposite to each other, and since $\mathbf{t}_{-y} = -\mathbf{t}_y$, the same work is done in both cases.

In some work the Burgers vector is defined by adopting the RH/FS convention, when it is obtained by connecting the points S and F, from the finishing point F to the starting point S of the Burgers circuit, i.e., **b** = **FS** (e.g., [12, p. 15]). The direction of the Burgers vector is then reversed in each part of Fig. 2. Furthermore, in this case,

$$\oint_C \mathrm{d}\mathbf{u} = -\mathbf{b}\,, \quad \oint_C \mathrm{d}u_x = b \tag{2.3}$$

and

$$\oint_C \mathrm{d}\mathbf{u} = -\mathbf{b}\,, \quad \oint_C \mathrm{d}u_x = -b \tag{2.4}$$

The specific work done by the traction $\mathbf{t}_\nu$ on the displacement discontinuity **b** across the cut surface is $-\mathbf{t}_\nu \cdot \mathbf{b}$, because the sliding surface Σ_1 translates by $-\mathbf{b}$ relative to the fixed surface Σ_2. This definition of the Burgers vector seems to be less convenient, at least in the context of the continuum elasticity theory, and will not be used further in this paper, although it has been frequently adopted in the literature on crystalline dislocations in materials science, e.g., Hertzberg [18, p. 60]; Smith and Hashemi [19, p. 157]; Askeland and Phulé [20, p. 93]. For crystalline dislocations, if the length of a Burgers vector is equal to one lattice spacing, the dislocation is referred to as a perfect dislocation (or dislocation of unit strength); if not, it is a partial dislocation. If energetically preferred, a perfect dislocation may dissociate into two partial dislocations, separated by a stacking fault, which is referred to as an extended dislocation (e.g., [21,10]).

2.1. *Burgers circuits for vertical cuts*

To facilitate the consideration of the dislocation loops in the next section, it is instructive to sketch the Burgers circuits around an edge dislocation, assumed to be created by the displacement discontinuity across the vertical cut, either above or below the dislocation. The extra half-sheet of material of thickness *b* (or the extra half-plane of atoms in the context of a crystalline dislocation) is either added or removed along the cut. In the first case the Burgers circuits are as shown in Fig. 3a and c, and in the second case as in Fig. 3b and d.

2.2. *Burgers vector of a dislocation loop*

Fig. 4 shows an idealized dislocation loop, formed by a pair of infinitely long, parallel positive and negative dislocations, at some distance from each other (the edge dislocation with the extra half-sheet of material above the dislocation is referred as the positive edge dislocation). In Fig. 4a, the displacement discontinuity *b* is imposed by sliding the surface Σ_1 above the horizontal cut, and in Fig. 4b by sliding the surface Σ_1 below the horizontal cut. Shown are the Burgers circuits around each dislocation, with the indicated direction of the dislocation line vector $\boldsymbol{\xi}$ along the loop (the loop is formally completed by two screw segments, connecting the edge segments and running out of the material at $z = \pm\infty$). Thus, the dislocation line direction $\boldsymbol{\xi}$ is into the plane of figure for one dislocation, and out of the plane of figure for the other dislocation. Figures 3c and 3d show the Burgers circuits for the dislocation loop created by the displacement discontinuity imposed along the vertical cut above the plane of the dislocation loop. Similar construction can be made for the dislocation loop created by the displacement discontinuity imposed along the vertical cut below the plane of the dislocation loop.

Fig. 5 shows a planar dislocation loop *C* created by imposing the displacement discontinuity along an arbitrary cut surface above the plane of the dislocation (Fig. 5a and b), or below that plane (Fig. 5c and d), with *C* as the boundary of the cut surface. Indicated are the Burgers circuits along the loop, dependent on the chosen line direction $\boldsymbol{\xi}$ along the loop. In particular, the cut surface may be taken to be a cylindrical surface emanating from *C* and exiting at the free surface of the body, either above or below the plane of the dislocation.

3. Peach–Koehler force – virtual work approach

Let us consider the dislocation loop shown in Fig. 6a, which resides in an infinite medium under remote loading. We will treat the most general case, in which the Burgers vector **b** is not in the plane of the loop. It is in the plane of the loop, the dislocation is referred to as a glide dislocation; if it is orthogonal to the plane of the loop, the dislocation is referred to as a prismatic or sessile dislocation. Imagine that the dislocation loop is created by imposing the displacement discontinuity **b** across the cut surface Σ below the loop, as shown in Fig. 6a. The work done on this displacement discontinuity (the

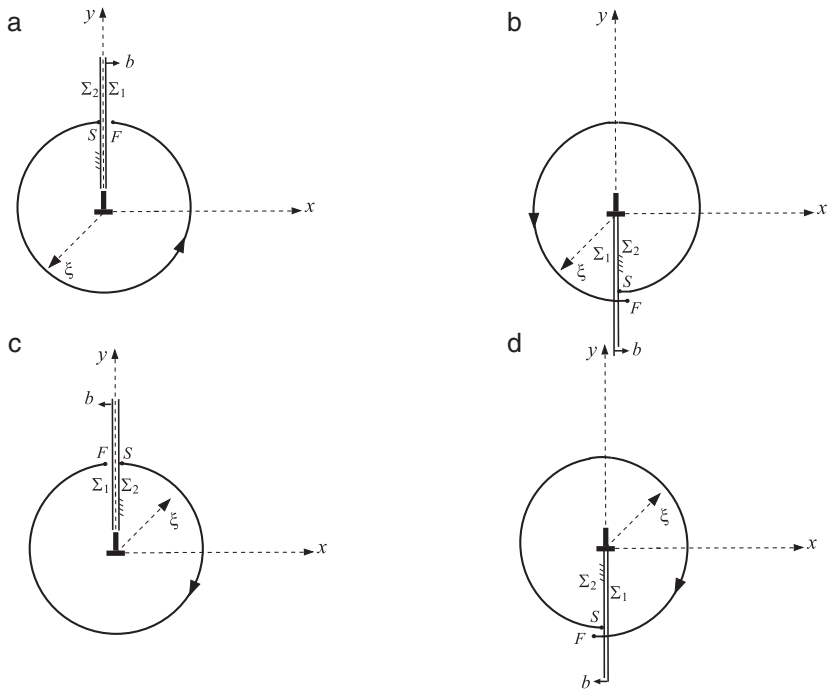

Fig. 3 – Same as Fig. 2 for the edge dislocation created by the displacement discontinuity *b* along the positive *y*-axis, parts (a) and (b), and negative *y*-axis, parts (c) and (d).

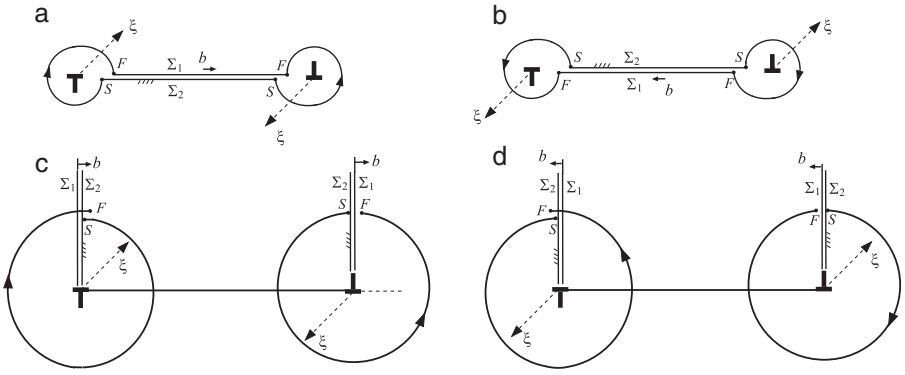

Fig. 4 – An idealized dislocation loop, formed by a pair of infinitely long, parallel positive and negative dislocations. In part (a), the displacement discontinuity *b* is imposed by sliding the surface Σ_1 above the horizontal cut, and in part (b) by sliding the surface Σ_1 below the horizontal cut. Shown are the Burgers circuits around each dislocation, with the indicated direction of the dislocation line vector ξ. Parts (c) and (d) are the same as parts (a) and (b), for the dislocation loop created by the displacement discontinuity along the vertical cuts.

interaction energy of the dislocation with the pre-existing stress field) is

$$W = \int_{\Sigma} \mathbf{t}_{\nu} \cdot \mathbf{b}\, d\Sigma\,, \quad \mathbf{t}_{\nu} = \boldsymbol{\sigma} \cdot \boldsymbol{\nu} = \boldsymbol{\nu} \cdot \boldsymbol{\sigma}\,, \tag{3.1}$$

where $\mathbf{t}_{\nu}$ is the traction vector over the surface Σ_1, whose unit normal $\boldsymbol{\nu}$ is directed toward Σ_2. The surface Σ_2 is considered fixed, while Σ_1 is displaced by the Burgers vector $\mathbf{b}$, as indicated in Fig. 5a. The stress tensor $\boldsymbol{\sigma}$ includes the stresses caused by remote loading or internal sources of stress, such as other dislocations (if present), but excludes the self-stress from the dislocation itself. Suppose that the dislocation loop evolves from its configuration C to a nearby configuration $C+\delta C$, by small displacements $\delta\mathbf{r}$ originating from the points of C (Fig. 6b). For simplicity, assume that both configurations are planar; the derivation for non-planar loops proceeds similarly. The dislocation loop in the configuration $C+\delta C$ can have a different size and shape from that in configuration C. The work done on creating the dislocation $C+\delta C$ is

$$W + \delta W = \int_{\Sigma+\delta\Sigma} \mathbf{t}_{\nu} \cdot \mathbf{b}\, d\Sigma = \int_{\Sigma} \mathbf{t}_{\nu} \cdot \mathbf{b}\, d\Sigma + \int_{\delta\Sigma} \mathbf{t}_{\nu} \cdot \mathbf{b}\, d(\delta\Sigma)\,. \tag{3.2}$$

We have conveniently used the surface $\Sigma+\delta\Sigma$ as the cut surface, with a cylindrical portion $\delta\Sigma$ as the surface between C

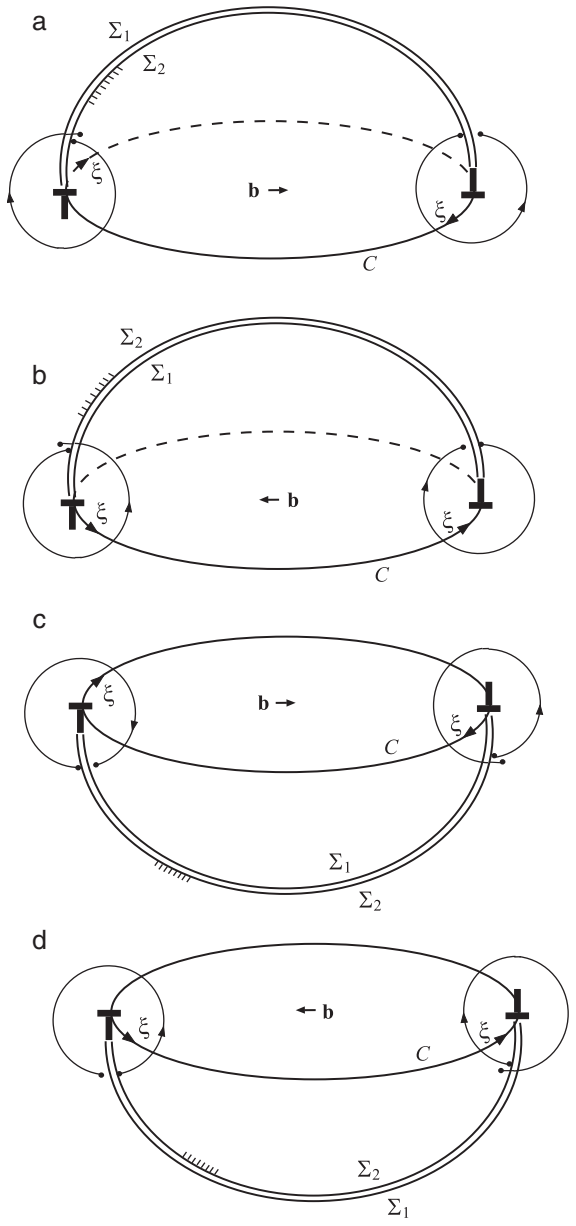

Fig. 5 – A planar dislocation loop C created by imposing the displacement discontinuity along an arbitrary cut surface above the plane of the dislocation, parts (a) and (b), or below that plane, parts (c) and (d). Indicated are the Burgers circuits along the loop, associated with the chosen direction of the line vector ξ along the loop. The surface Σ_2 is considered fixed, while Σ_1 is displaced by b.

and $C+\delta C$. Thus, the work done on the transformation of the loop from C to $C+\delta C$ is

$$\delta W = \int_{\delta\Sigma} \mathbf{t}_\nu \cdot \mathbf{b}\, \mathrm{d}(\delta\Sigma)\,. \tag{3.3}$$

The configurational force (per unit length of the dislocation) **f** is defined so that its work on the displacement $\delta\mathbf{r}$ along the loop is equal to $-\delta W$, i.e.,

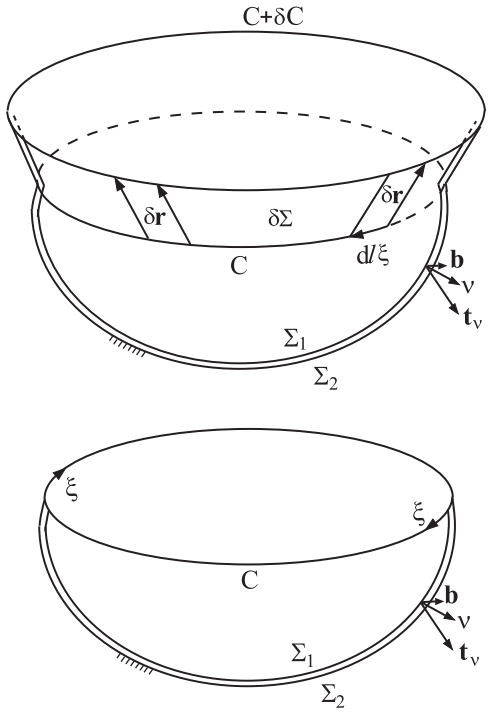

Fig. 6 – (a) The dislocation loop C created by a cut surface below its plane. The surface Σ_1 is displaced by the Burgers vector b, while the surface Σ_2 is considered fixed. The traction vector over Σ_1 is $\mathbf{t}_\nu$, where ν is the unit vector orthogonal to Σ_1 and directed towards Σ_2. (b) A nearby configuration of the dislocation loop $C+\delta C$, obtained from C by the displacement variation $\delta\mathbf{r}$ originating from points of C. The surface connecting C and $C+\delta C$ is $\delta\Sigma$. The arc length of C is denoted by dl.

$$\oint_C (\mathbf{f}\cdot\delta\mathbf{r})\,\mathrm{d}l = -\delta W\,. \tag{3.4}$$

The negative sign in front of δW is used, because if the dislocation loop spontaneously moves from its configuration C to $C+\delta C$, the corresponding energy must decrease ($\delta W<0$).

The objective is now to derive an explicit expression for **f** along the dislocation loop, in terms of the stress field $\boldsymbol{\sigma}$ and the dislocation Burgers vector **b**. This can be accomplished by comparing (3.3) and (3.4). The substitution of the Cauchy relation $\mathbf{t}_\nu = \boldsymbol{\sigma}\cdot\boldsymbol{\nu}$ into (3.3) gives

$$\delta W = \int_{\delta\Sigma} (\boldsymbol{\sigma}\cdot\mathbf{b})\cdot \mathrm{d}(\delta\boldsymbol{\Sigma})\,, \quad \mathrm{d}(\delta\boldsymbol{\Sigma}) = \boldsymbol{\nu}\,\mathrm{d}(\delta\Sigma)\,. \tag{3.5}$$

From the sketch in Fig. 6b, the vectorial surface element along $\delta\Sigma$ is $\mathrm{d}(\delta\boldsymbol{\Sigma}) = \delta\mathbf{r}\times(\boldsymbol{\xi}\,\mathrm{d}l)$, where $\boldsymbol{\xi}$ is the unit vector along the dislocation line, and $\mathrm{d}l$ is the length element of this line. The unit normal $\boldsymbol{\nu}$ is directed from $\delta\Sigma_1$ to $\delta\Sigma_2$. The substitution of this expression into (3.5) gives

$$\delta W = \oint_C \delta\mathbf{r}\cdot[\boldsymbol{\xi}\times(\boldsymbol{\sigma}\cdot\mathbf{b})]\,\mathrm{d}l\,. \tag{3.6}$$

The cyclic property of the triple-vector product is used giving $(\boldsymbol{\sigma}\cdot\mathbf{b})\cdot(\delta\mathbf{r}\times\boldsymbol{\xi})=\delta\mathbf{r}\cdot[\boldsymbol{\xi}\times(\boldsymbol{\sigma}\cdot\mathbf{b})]$. The comparison of (3.6) with (3.4) establishes the well-known Peach–Koehler [5] expression for the dislocation force

$$\mathbf{f}=(\boldsymbol{\sigma}\cdot\mathbf{b})\times\boldsymbol{\xi}\,. \tag{3.7}$$

Being defined by the cross product of the vectors $(\boldsymbol{\sigma}\cdot\mathbf{b})$ and $\boldsymbol{\xi}$, the force $\mathbf{f}$ is orthogonal to the dislocation line vector $\boldsymbol{\xi}$ at each point of the loop. In the index notation, with respect to an orthogonal Cartesian coordinate system, the components of the dislocation force are

$$f_k=\epsilon_{kij}\sigma_{il}b_l\xi_j\,,\quad (k=1,2,3)\,, \tag{3.8}$$

where ϵ_{kij} are the components of the permutation tensor. An alternative derivation, also in the spirit of virtual work consideration, with an arbitrary infinitesimal variation of the dislocation configuration, was used by Gavazza and Barnett [22], Hirth and Lothe [8, p. 109], and Eshelby [14]. See also Asaro and Lubarda [23, p. 365], and Balluffi [15, pp. 415 and 453].

In the expression (3.7), the adopted convention for the direction of the Burgers vector $\mathbf{b}$ and the corresponding direction of the dislocation line vector $\boldsymbol{\xi}$ need to be carefully used. The same dislocation force is obtained from (3.7) by adopting either of the conventions shown in Fig. 5c and d, because $\mathbf{b}$ and $\boldsymbol{\xi}$ in Fig. 5d are opposite in direction to those in Fig. 5c. Sign errors in the expression for the dislocation force were pointed out and discussed by de Wit [13], and Hirth and Lothe [8, p. 91]. Nabarro [24] derived the dislocation force expression in the form equivalent to $\mathbf{f}=\boldsymbol{\xi}\times(\boldsymbol{\sigma}\cdot\mathbf{b})$ (see his Eq. (2.66) on p. 83), which thus predicts the opposite direction of the force to that predicted by (3.7). This resulted from his omission of the negative sign on the right-hand side of (3.4). The same comment applies to the derivation used in Lubarda [25]. On the other hand, Weertman and Weertman [12] derive the expression $\mathbf{f}=\boldsymbol{\xi}\times(\boldsymbol{\sigma}\cdot\mathbf{b})$ (Eq. (3.20) on p. 61), but their definition of the direction of the Burgers vector is opposite to that used in (3.7), while the direction of the dislocation line vector $\boldsymbol{\xi}$ is the same in both cases, so that the two seemingly different expressions predict the same magnitude and direction of the dislocation force.

The direction of the dislocation line vector is also important in understanding how the loops in the Frank–Read source punch-off by attraction of their parallel screw segments [18,70]. One would at first think that they repel each other because the segments have the same Burgers vector, that of the entire loop, and are in the same plane. However, closer inspection reveal that dislocation line vectors of two screw segments have opposite senses ($\boldsymbol{\xi}_2=-\boldsymbol{\xi}_1$), and thus two segments attract each other as two opposite screw dislocations (Fig. 7).

3.1. *Glide and climb components of the dislocation force*

Fig. 8 shows a planar dislocation loop C within the plane whose unit normal is $\mathbf{n}=\boldsymbol{\xi}\times\mathbf{m}$, where $\mathbf{m}$ is the unit vector in the plane of the loop, orthogonal to the loop and directed outward from it. The projections of $\mathbf{f}$ onto $\mathbf{m}$ and $\mathbf{n}$ are then

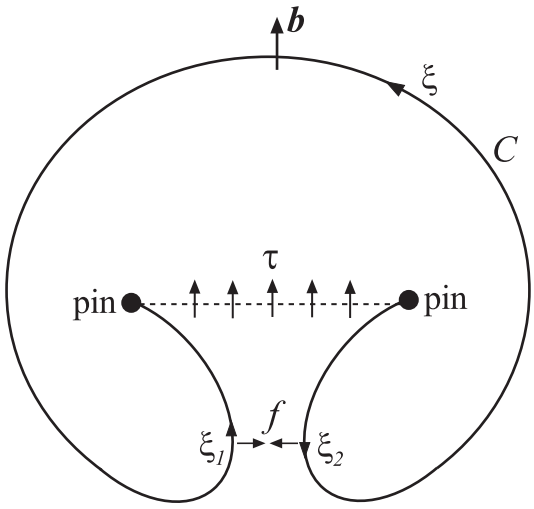

Fig. 7 – A Frank–Read dislocation source: bowing out loop from a pinned dislocation segment (shown dashed) under applied shear stress τ. The two nearby screw segments attract each other because their local dislocation line vectors are $\boldsymbol{\xi}_1\sim\mathbf{b}$ and $\boldsymbol{\xi}_2\sim-\mathbf{b}$, such that $\boldsymbol{\xi}_2=-\boldsymbol{\xi}_1$.

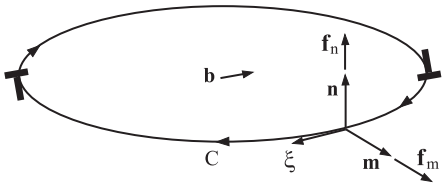

Fig. 8 – A planar dislocation loop C within the plane whose unit normal is $\mathbf{n}=\boldsymbol{\xi}\times\mathbf{m}$, where $\mathbf{m}$ is the unit vector in the plane of the loop, orthogonal to it and directed outward from it. The dislocation Burgers vector is $\mathbf{b}$, which is not necessarily within the plane of the loop. The projections of the dislocation force $\mathbf{f}$ onto $\mathbf{m}$ and $\mathbf{n}$ are f_m and f_n.

$$f_m=\mathbf{f}\cdot\mathbf{m}=[(\boldsymbol{\sigma}\cdot\mathbf{b})\times\boldsymbol{\xi}]\cdot\mathbf{m}=(\mathbf{b}\cdot\boldsymbol{\sigma})\cdot(\boldsymbol{\xi}\times\mathbf{m})=\mathbf{b}\cdot\boldsymbol{\sigma}\cdot\mathbf{n}=\mathbf{t}_n\cdot\mathbf{b}\,, \tag{3.9}$$

and

$$f_n=\mathbf{f}\cdot\mathbf{n}=[(\boldsymbol{\sigma}\cdot\mathbf{b})\times\boldsymbol{\xi}]\cdot\mathbf{n}=(\mathbf{b}\cdot\boldsymbol{\sigma})\cdot(\boldsymbol{\xi}\times\mathbf{n})=-\mathbf{b}\cdot\boldsymbol{\sigma}\cdot\mathbf{m}=-\mathbf{t}_m\cdot\mathbf{b}\,. \tag{3.10}$$

The projection f_ξ is equal to zero, because the dislocation force $\mathbf{f}$ is orthogonal to $\boldsymbol{\xi}$.

If the Burgers vector $\mathbf{b}$ is decomposed into its components within the plane of the dislocation loop and orthogonal to it ($\mathbf{b}=b_\xi\boldsymbol{\xi}+b_m\mathbf{m}+b_n\mathbf{n}$), it readily follows from (3.9) and (3.10) that

$$f_m=\sigma_{n\xi}b_\xi+\sigma_{nm}b_m+\sigma_{nn}b_n\,,\quad f_n=-(\sigma_{m\xi}b_\xi+\sigma_{mm}b_m+\sigma_{mn}b_n)\,. \tag{3.11}$$

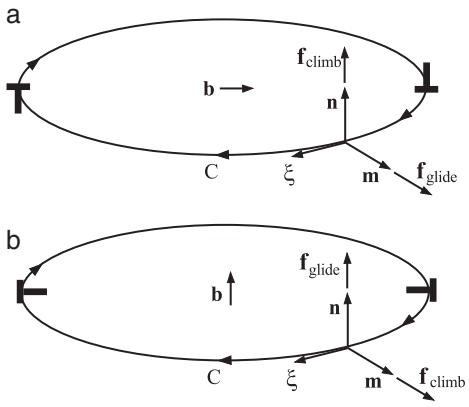

Fig. 9 – (a) A glide dislocation loop, with the Burgers vector b in the plane of the loop. The glide and climb components of the dislocation force are f_m and f_n, respectively. (b) A sessile dislocation loop, with the Burgers vector b orthogonal to the plane of the loop. The glide and climb components of the dislocation force are f_n and f_m, respectively.

The Burgers vector component b_ξ is the screw component of the dislocation at a given point of the dislocation loop, while b_m and b_n are its edge components, within the plane of the loop and orthogonal to it. The stress tensor components used in (3.11) are defined with respect to the local coordinate system ($\boldsymbol{\xi}$, **m**, **n**).

For example, if the dislocation is a glide dislocation ($b_n = 0$, Fig. 9a), the glide and climb forces are

$$f_{\text{glide}} = f_m = \sigma_{n\xi} b_\xi + \sigma_{nm} b_m\,, \quad f_{\text{climb}} = f_n = -(\sigma_{m\xi} b_\xi + \sigma_{mm} b_m)\,. \tag{3.12}$$

We can also write $\mathbf{f} = \mathbf{f}_{\text{glide}} + \mathbf{f}_{\text{climb}}$, with $\mathbf{f}_{\text{glide}} = (\mathbf{f}\cdot\mathbf{m})\mathbf{m}$ and $\mathbf{f}_{\text{climb}} = (\mathbf{f}\cdot\mathbf{n})\mathbf{n}$. The vectors **n** and **m** can be expressed solely in terms of the coplanar vectors $\boldsymbol{\xi}$ and **b** as

$$\mathbf{m} = \frac{\boldsymbol{\xi}\times(\mathbf{b}\times\boldsymbol{\xi})}{|\mathbf{b}\times\boldsymbol{\xi}|}\,, \quad \mathbf{n} = \boldsymbol{\xi}\times\mathbf{m}\,. \tag{3.13}$$

It is noted that the screw and edge components of the glide dislocation at the considered point of the loop are $\mathbf{b}_{\text{screw}} = (\mathbf{b}\cdot\boldsymbol{\xi})\boldsymbol{\xi}$ and $\mathbf{b}_{\text{edge}} = (\mathbf{b}\cdot\mathbf{m})\mathbf{m} \equiv (\boldsymbol{\xi}\times\mathbf{b})\times\boldsymbol{\xi}$. See also Cai and Nix [9, p. 270], and Anderson et al. [10, p. 80].

For a sessile (prismatic) dislocation loop ($b_\xi = b_m = 0$, $b_n = b$, Fig. 9b), the glide and climb forces are

$$f_{\text{glide}} = f_n = -\sigma_{mn} b_n\,, \quad f_{\text{climb}} = f_m = \sigma_{nn} b_n\,. \tag{3.14}$$

3.2. *Circular dislocation loop*

For a circular dislocation loop in the (x, y) plane whose Burgers vector is $\mathbf{b} = \{\cos\varphi, \sin\varphi, 0\}$, with respect to (x, y, z) coordinate system, the glide and climb forces at the point of the loop specified by the polar angle θ are

$$\begin{aligned} f_{\text{glide}} &= f_r = \sigma_{zr} b_r + \sigma_{z\theta} b_\theta = [\sigma_{zr}\cos(\varphi-\theta) + \sigma_{z\theta}\sin(\varphi-\theta)]b\,,\\ f_{\text{climb}} &= f_z = -(\sigma_{rr} b_r + \sigma_{r\theta} b_\theta) = -[\sigma_{rr}\cos(\varphi-\theta) + \sigma_{r\theta}\sin(\varphi-\theta)]b\,. \end{aligned} \tag{3.15}$$

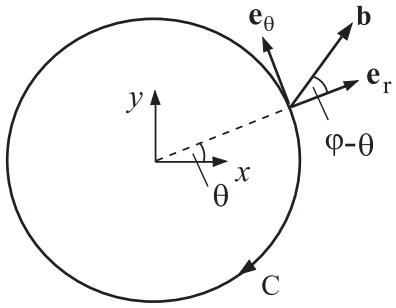

Fig. 10 – A circular dislocation loop with the Burgers vector $\mathbf{b} = \{\cos\varphi, \sin\varphi, 0\}$, relative to the (x, y, z) coordinate system. The angle between the Burgers vector and the x-axis is φ. The in-plane polar coordinates are (r, θ), with the corresponding unit vectors ($\mathbf{e}_r$, $\mathbf{e}_\theta$).

In these expressions, the components of the Burgers vector with respect to polar coordinates (r, θ) are $b_r = b\cos(\varphi-\theta)$ and $b_\theta = b\sin(\varphi-\theta)$ (Fig. 10). For example, if the only non-vanishing stress components in the (x, y, z) coordinate system are σ_{zx} and σ_{xx}, and if $\varphi = 0$ (i.e., $b = b_x$), the glide and climb forces are

$$f_{\text{glide}} = f_r = \sigma_{zx} b\,, \quad f_{\text{climb}} = f_z = -\sigma_{xx} b\cos\theta\,. \tag{3.16}$$

For a sessile circular dislocation loop in the (x, y) plane, with the Burgers vector $\mathbf{b} = \{0, 0, b\}$, the glide and climb forces are

$$f_{\text{glide}} = f_z = -\sigma_{zr} b = -(\sigma_{zx}\cos\theta + \sigma_{zy}\sin\theta)b\,, \quad f_{\text{climb}} = f_r = \sigma_{zz} b\,. \tag{3.17}$$

3.3. *Corner forces*

If a dislocation loop has a sharp corner, the contributions to the dislocation force from smooth sides of the loop vectorially add at the corner. For example, for a sessile rectangular dislocation loop with the Burgers vector b_z along the z-direction, orthogonal to the plane of the loop (Fig. 11), the total glide force at each corner is $F_{\text{glide}} = (\sigma_{xz} + \sigma_{yz})b_z$, directed vertically downwards, while the total climb force is $F_{\text{climb}} = \sqrt{2}\sigma_{zz} b_z$, at 45° inbetween (x, y) directions.

3.4. *Osmotic (chemical) force on a dislocation*

The motion of a crystalline dislocation within its glide plane under applied stress is opposed by the lattice friction. This is often represented by the Peirles-Nabarro stress $\tau_{\text{PN}} = G\exp(2\pi w/b)$, where G is the shear modulus and w is the so-called width of the dislocation, which, in certain sense, accounts for the dislocation core spreading [26,27,24]. The dislocation motion orthogonal to its glide plane is opposed by the barriers to atomic diffusion, because a dislocation can move out of its plane only if the point defects (e.g., vacancies) diffuse to or away from the dislocation, assuming that the temperature of the material is sufficiently high for rapid diffusion [12]. In the absence of applied stress, and at a given temperature T, there is an equilibrium concentration of vacancies (c_0)

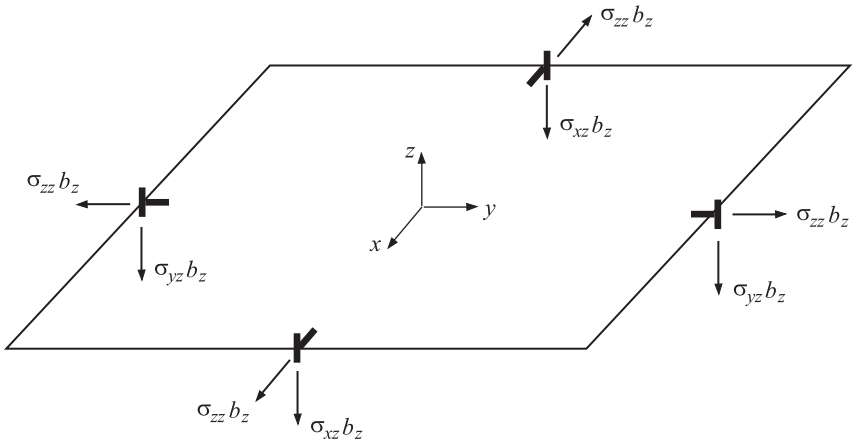

Fig. 11 – A sessile rectangular dislocation loop with the Burgers vector b_z, orthogonal to the (x, y) plane of the loop. Shown are the glide and climb forces along smooth parts of the loop, which vectorially add at the corner.

at which a dislocation is in equilibrium and does not move out of its glide plane. Under applied stress, the climb component of the Peach-Koehler force pushes a dislocation to move orthogonal to its glide plane. If a positive edge dislocation of a Burgers vector b_x is under tensile stress σ_{xx}, it can move downwards by absorbing the surrounding atoms from a lattice to extend its extra half plane, which increases the concentration of vacancies (c) around the dislocation. The dislocation motion becomes more difficult as the vacancy concentration increases, approaching its equilibrium concentration, corresponding to given level of applied stress σ_{xx}, when dislocation motion stops. Based on the analysis of the Gibbs free energy, it can be shown that the opposing, osmotic or chemical force to stress-driven dislocation climb is due to the excess concentration of vacancies [12,28,10]. This force is $\mathbf{f}_{os} = f_{os}\mathbf{n}$, where $\mathbf{n}$ is a unit vector orthogonal to the glide plane, and

$$f_{os} = \frac{kTb_e}{v_a} \ln \frac{c}{c_0}. \tag{3.18}$$

The Boltzmann constant is k, and v_a is the atomic volume. The osmotic force is zero at $c = c_0$, but it logarithmically increases as $c \to c_{eq}$, as it becomes harder to absorb new atoms from a vacancy more saturated lattice surrounding the dislocation.

If the climb component of the Peach-Koehler force due to mechanical stress is $\mathbf{f}_{cl} = f_{cl}\mathbf{n}$, the dislocation will be in equilibrium with respect to the motion out of its glide plane if $f_{cl} + f_{os} = 0$, i.e.,

$$f_{cl} + \frac{kTb_e}{v_a} \ln \frac{c_{eq}}{c_0} = 0. \tag{3.19}$$

This specifies the equilibrium vacancy concentration corresponding to a given stress state

$$c_{eq} = c_0 \exp\left(-\frac{f_{cl} v_a}{kTb_e}\right). \tag{3.20}$$

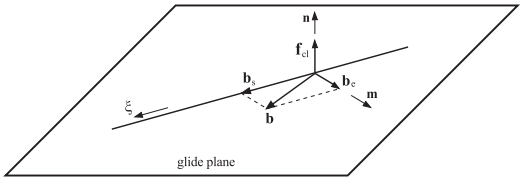

Fig. 12 – An infinitely long straight dislocation along the ξ direction. The Burgers vector of dislocation b is within a glide plane whose unit normal is n. The edge and screw components of the Burgers vector are $\mathbf{b}_e$ and $\mathbf{b}_s$. The climb component of the dislocation force is $\mathbf{f}_{cl}$.

For example, for a straight dislocation with a Burgers vector $\mathbf{b}$ within a glide plane whose unit normal is $\mathbf{n}$ (Fig. 12), the climb force is

$$f_{cl} = \mathbf{f} \cdot \mathbf{n}, \quad \mathbf{f} = (\boldsymbol{\sigma} \cdot \mathbf{b}) \times \boldsymbol{\xi}. \tag{3.21}$$

The unit vector along the dislocation line is $\boldsymbol{\xi}$, and

$$\mathbf{n} = \frac{\boldsymbol{\xi} \times \mathbf{b}}{|\boldsymbol{\xi} \times \mathbf{b}|}, \quad \mathbf{m} = \mathbf{n} \times \boldsymbol{\xi}. \tag{3.22}$$

The edge component of the Burgers vector is (cf. expression (15.80) of [10])

$$b_e = \mathbf{b} \cdot \mathbf{m} = \mathbf{b} \cdot (\mathbf{n} \times \boldsymbol{\xi}) = \mathbf{b} \cdot \frac{(\boldsymbol{\xi} \times \mathbf{b}) \times \boldsymbol{\xi}}{|\boldsymbol{\xi} \times \mathbf{b}|}. \tag{3.23}$$

In particular, if $\boldsymbol{\xi} = \mathbf{e}_z$, $\mathbf{n} = \mathbf{e}_y$, and $\mathbf{b} = b_x\mathbf{e}_x + b_z\mathbf{e}_z$, while $\boldsymbol{\sigma} = \sigma_{xx}\mathbf{e}_x \otimes \mathbf{e}_x$, where $\otimes$ denotes the dyadic product, it follows from (3.21) that $f_{cl} = -\sigma_{xx}b_x$, and (3.20) reduces to $c_{eq} = c_0 \exp[(\sigma_{xx}v_a)/(kT)]$.

4. Derivation of the Peach–Koehler force by the potential energy consideration

A more general analysis, which allows for the incorporation of the contribution of the image stresses to the dislocation

force, is based on the consideration of the potential energy. This analysis is in the spirit of the Eshelby's [29,30] approach, which gave birth to the field of mechanics known today as the configurational mechanics. The potential energy of the loaded body with a dislocation loop inside of it is defined as the difference of the strain energy U stored in the body and the load potential P, i.e.,

$$\Pi = U - P\,. \tag{4.1}$$

If $\mathbf{t}_n^0$ is the applied traction over the bounding surface S of the body, with $\mathbf{n}$ being the outward unit vector orthogonal to S, the load potential is

$$P = \int_S \mathbf{t}_n^0 \cdot (\mathbf{u}^0 + \mathbf{u}^{\mathrm{d}})\,\mathrm{d}S\,. \tag{4.2}$$

The displacement vector due to external load is denoted by $\mathbf{u}^0$, and that due to the dislocation loop alone is $\mathbf{u}^{\mathrm{d}}$.

The total strain energy within the body of volume V is $U = U^0 + U^{\mathrm{d}}$. The part of the strain energy due to applied load is

$$U^0 = \frac{1}{2}\int_V \boldsymbol{\sigma}^0 : \boldsymbol{\epsilon}^0\,\mathrm{d}V, \tag{4.3}$$

where $\boldsymbol{\sigma}^0$ and $\boldsymbol{\epsilon}^0$ are the stress and strain fields induced by $\mathbf{t}_n^0$, and : stands for the trace product. The strain energy due to dislocation alone is U^{d}. The additive representation $U = U^0 + U^{\mathrm{d}}$ holds, because the well-known theorem of linear elasticity [8, p. 53] states that there is no interaction strain energy between the self-equilibrating stress field due to internal source of stress (such as dislocation) and the strain field due to externally applied load.

The dislocation strain energy U^{d} is represented as the sum of the core energy $U_{\mathrm{c}}^{\mathrm{d}}$ within the volume V_{c} of a narrow tube surrounding the dislocation line (along which the linear elasticity predicts singular stresses), and the strain energy within the volume $V - V_{\mathrm{c}}$, outside of this tube, i.e.,

$$U^{\mathrm{d}} = U_{\mathrm{c}}^{\mathrm{d}} + \frac{1}{2}\int_{V-V_{\mathrm{c}}} \boldsymbol{\sigma}^{\mathrm{d}} : \boldsymbol{\epsilon}^{\mathrm{d}}\,\mathrm{d}V\,. \tag{4.4}$$

The stress and strain fields due to the dislocation alone in the externally unloaded body are denoted by $\boldsymbol{\sigma}^{\mathrm{d}}$ and $\boldsymbol{\epsilon}^{\mathrm{d}}$. Since linear elasticity predicts infinitely large core energy, nonlinear or other theory is needed to specify $U_{\mathrm{c}}^{\mathrm{d}}$, which is beyond the scope of this paper ([31,32]). An alternative construction of the potential energy functional, based on the Kröner [6] decomposition of strain into its (incompatible) elastic and plastic (localized, slip induced) parts, was used by Mura [33, p. 353], and Le [34, p. 115]. See also Balluffi [15, p. 337].

As commonly done in the dislocation studies [29,30,14,8,35,22,36,25,37,9], the stress and strain fields of the dislocation in a finite body is represented as the sum of the infinite-medium stress and strain fields ($\tilde{\boldsymbol{\sigma}}$ and $\tilde{\boldsymbol{\epsilon}}$) and the image fields ($\hat{\boldsymbol{\sigma}}$ and $\hat{\boldsymbol{\epsilon}}$), needed to make the boundary of the finite body traction-free, i.e., $\boldsymbol{\sigma}^{\mathrm{d}} = \tilde{\boldsymbol{\sigma}} + \hat{\boldsymbol{\sigma}}$ and $\boldsymbol{\epsilon}^{\mathrm{d}} = \tilde{\boldsymbol{\epsilon}} + \hat{\boldsymbol{\epsilon}}$. This

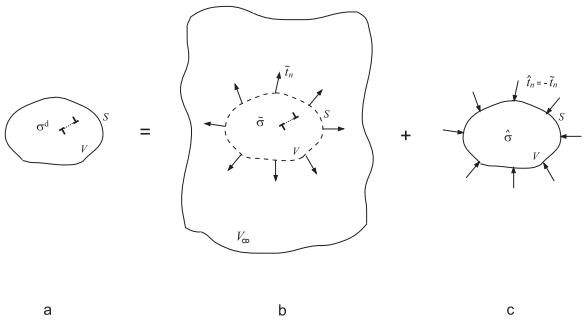

Fig. 13 – The stress field σ^{d} of the dislocation in a finite body of volume V, whose boundary S is traction-free is represented as the sum of the infinite-medium stress field ($\tilde{\sigma}$) and the image stress field ($\hat{\sigma}$). The image field is due to the traction $\hat{\mathbf{t}}_n = -\tilde{\mathbf{t}}_n$ applied over S in the configuration (c) to cancel the traction $\tilde{\mathbf{t}}_n$ induced over S by the infinite-medium field in part (b).

superposition is sketched in Fig. 13. It readily follows from (4.4) that

$$U^{\mathrm{d}} = \tilde{U}_{\mathrm{c}} + \frac{1}{2}\int_{V-V_{\mathrm{c}}} \tilde{\boldsymbol{\sigma}} : \tilde{\boldsymbol{\epsilon}}\,\mathrm{d}V + \frac{1}{2}\int_V \hat{\boldsymbol{\sigma}} : \tilde{\boldsymbol{\epsilon}}\,\mathrm{d}V\,. \tag{4.5}$$

The reciprocity property $\tilde{\boldsymbol{\sigma}} : \hat{\boldsymbol{\epsilon}} = \hat{\boldsymbol{\sigma}} : \tilde{\boldsymbol{\epsilon}}$ was used, together with the vanishing of the integral $\int_V \boldsymbol{\sigma}^{\mathrm{d}} : \hat{\boldsymbol{\epsilon}}\,\mathrm{d}V = 0$, which follows from the Gauss divergence theorem and the zero traction $\mathbf{t}_n^{\mathrm{d}}$ over S. The core energy of the dislocation in an infinite medium is denoted in (4.5) by $\tilde{U}_{\mathrm{c}}$.

The third term on the right-hand side of (4.5) can be expressed by the Gauss divergence theorem as

$$\frac{1}{2}\int_V \hat{\boldsymbol{\sigma}} : \tilde{\boldsymbol{\epsilon}}\,\mathrm{d}V = \frac{1}{2}\int_S \hat{\mathbf{t}}_n \cdot \tilde{\mathbf{u}}\,\mathrm{d}S + \frac{1}{2}\int_\Sigma \hat{\mathbf{t}}_\nu \cdot \mathbf{b}\,\mathrm{d}\Sigma\,, \tag{4.6}$$

where $\tilde{\mathbf{u}}$ is the displacement of the ˜ field. The product $\hat{\mathbf{t}}_\nu \cdot \mathbf{b}$ represents the specific work of the traction $\hat{\mathbf{t}}_\nu = \hat{\boldsymbol{\sigma}} \cdot \boldsymbol{\nu}$ on the displacement discontinuity $\mathbf{b}$ over the cut surface Σ used to create the dislocation loop. The unit normal $\boldsymbol{\nu}$ is orthogonal to the surface Σ_1 and directed towards the surface Σ_2, as elaborated upon in Section 2.2. Furthermore, we can write

$$\frac{1}{2}\int_{V-V_{\mathrm{c}}} \tilde{\boldsymbol{\sigma}} : \tilde{\boldsymbol{\epsilon}}\,\mathrm{d}V = \frac{1}{2}\int_{V_\infty - V_{\mathrm{c}}} \tilde{\boldsymbol{\sigma}} : \tilde{\boldsymbol{\epsilon}}\,\mathrm{d}V - \frac{1}{2}\int_{V_\infty - V} \tilde{\boldsymbol{\sigma}} : \tilde{\boldsymbol{\epsilon}}\,\mathrm{d}V\,, \tag{4.7}$$

where V_∞ denotes the volume of the entire infinite medium. By the Gauss divergence theorem, the second integral on the right-hand side of (4.7) is

$$\frac{1}{2}\int_{V_\infty - V} \tilde{\boldsymbol{\sigma}} : \tilde{\boldsymbol{\epsilon}}\,\mathrm{d}V = \frac{1}{2}\int_S \hat{\mathbf{t}}_n \cdot \tilde{\mathbf{u}}\,\mathrm{d}S\,, \tag{4.8}$$

because the self-equilibrating traction $\hat{\mathbf{t}}_n = \tilde{\mathbf{t}}_{-n}$ acts on the bounding surface S of the volume $V_\infty - V$ (Fig. 14). The corresponding stress and displacement at infinity rapidly diminish and do not contribute any work over the infinitely remote boundary on the right-hand side of (4.8).

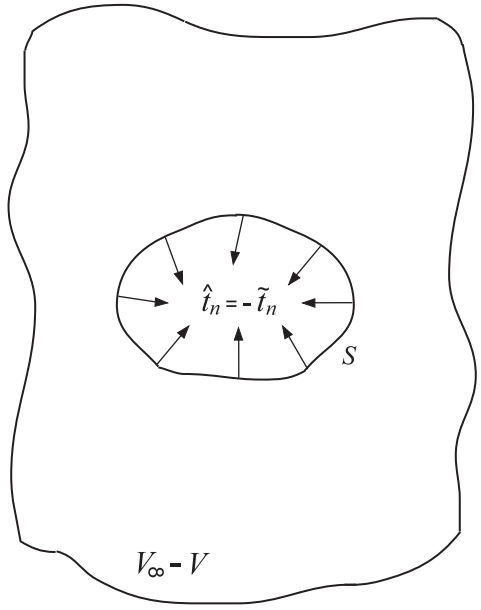

Fig. 14 – The surface S of the hole in the dislocation-free infinite medium under the traction $\hat{\mathbf{t}}_n = -\tilde{\mathbf{t}}_n$.

By combining (4.6)–(4.8), the substitution into (4.5) gives the following expression for the dislocation strain energy

$$U^{\mathrm{d}} = \tilde{U}_{\mathrm{c}} + \tilde{U}_{\infty-\mathrm{c}} + \frac{1}{2}\int_{\Sigma} \hat{\mathbf{t}}_{\nu}\cdot\mathbf{b}\,\mathrm{d}\Sigma\,, \quad \tilde{U}_{\infty-\mathrm{c}} = \frac{1}{2}\int_{V_\infty - V_{\mathrm{c}}} \tilde{\boldsymbol{\sigma}} : \tilde{\boldsymbol{\epsilon}}\,\mathrm{d}V\,. \tag{4.9}$$

The dislocation strain energy in the infinite medium outside the dislocation core is denoted by $\tilde{U}_{\infty-\mathrm{c}}$, so that the first two terms on the right-hand side of (4.9) represent the entire strain energy of the dislocation loop in the infinite medium (self-energy of the dislocation loop). The third term is the correction from the image traction needed to achieve the traction-free boundary condition for the dislocation embedded in the finite body of volume V.

In view of (4.2) and (4.3), the total potential energy (4.1) can now be expressed as

$$\Pi = \Pi^0 + U^{\mathrm{d}} - \int_S \mathbf{t}^0_n\cdot\mathbf{u}^{\mathrm{d}}\,\mathrm{d}S\,, \tag{4.10}$$

where

$$\Pi^0 = U^0 - \int_S \mathbf{t}^0_n\cdot\mathbf{u}^0\,\mathrm{d}S \tag{4.11}$$

is the potential energy of the loaded body without a dislocation. Furthermore, we have

$$\int_S \mathbf{t}^0_n\cdot\mathbf{u}^{\mathrm{d}}\,\mathrm{d}S = -\int_\Sigma \mathbf{t}^0_\nu\cdot\mathbf{b}\,\mathrm{d}\Sigma\,, \tag{4.12}$$

which follows from the reciprocity $\boldsymbol{\sigma}^0 : \boldsymbol{\epsilon}^{\mathrm{d}} = \boldsymbol{\sigma}^{\mathrm{d}} : \boldsymbol{\epsilon}^0$, the traction-free dislocation boundary condition $\mathbf{t}^{\mathrm{d}} = 0$, and the Gauss divergence theorem applied to $\int_V \boldsymbol{\sigma}^0 : \boldsymbol{\epsilon}^{\mathrm{d}}\,\mathrm{d}V = 0$. Thus, by incorporating (4.9) and (4.12) into (4.10), the potential energy becomes

$$\Pi = \Pi^0 + \tilde{U}_{\mathrm{c}} + \tilde{U}_{\infty-\mathrm{c}} + \frac{1}{2}\int_\Sigma \hat{\mathbf{t}}_\nu\cdot\mathbf{b}\,\mathrm{d}\Sigma + \int_\Sigma \mathbf{t}^0_\nu\cdot\mathbf{b}\,\mathrm{d}\Sigma\,. \tag{4.13}$$

Although this aspect of the analysis will not be pursued further in this paper, the strain energy $\tilde{U}_{\infty-\mathrm{c}}$ can also be expressed by the Gauss divergence theorem as

$$\tilde{U}_{\infty-\mathrm{c}} = \frac{1}{2}\int_{V_\infty - V_{\mathrm{c}}} \tilde{\boldsymbol{\sigma}} : \tilde{\boldsymbol{\epsilon}}\,\mathrm{d}V = \frac{1}{2}\int_{S_{\mathrm{c}}} \tilde{\mathbf{t}}^{\mathrm{c}}_n\cdot\tilde{\mathbf{u}}^{\mathrm{c}}\,\mathrm{d}S_{\mathrm{c}} + \frac{1}{2}\int_\Sigma \tilde{\mathbf{t}}_\nu\cdot\mathbf{b}\,\mathrm{d}\Sigma\,. \tag{4.14}$$

Such representation is of great importance in the evaluation of the self-force on the dislocation (from the dislocation itself), as demonstrated by Gavazza and Barnett [22]; see also Eshelby [14]. The traction and displacement components over the core surface S_{c} are denoted in (4.14) by $\tilde{\mathbf{t}}^{\mathrm{c}}_n$ and $\tilde{\mathbf{u}}^{\mathrm{c}}$. As pointed out by Gavazza and Barnett [22], while $\tilde{U}_{\infty-\mathrm{c}}$ is independent of the choice of the cut surface, the two individual contributions (from the surface integrals over S_{c} and Σ) on the right-hand side of (4.14) do depend on the cut surface over which the displacement discontinuity is imposed. In the two-dimensional context of straight dislocations, this was further elaborated upon by Lubarda [38].

4.1. *Variation of the potential energy*

The variation of the potential energy (4.13) is

$$\delta\Pi = \delta\Pi^0 + \delta\tilde{U}_{\mathrm{c}} + \delta\tilde{U}_{\infty-\mathrm{c}} + \int_{\delta\Sigma} (\mathbf{t}^0_\nu + \hat{\mathbf{t}}_\nu)\cdot\mathbf{b}\,\mathrm{d}(\delta\Sigma)\,, \tag{4.15}$$

where we have used the result [39]

$$\delta\int_\Sigma \hat{\mathbf{t}}_\nu\cdot\mathbf{b}\,\mathrm{d}\Sigma = \int_\Sigma \delta\hat{\mathbf{t}}_\nu\cdot\mathbf{b}\,\mathrm{d}\Sigma + \int_{\delta\Sigma} \hat{\mathbf{t}}_\nu\cdot\mathbf{b}\,\mathrm{d}(\delta\Sigma) = 2\int_{\delta\Sigma} \hat{\mathbf{t}}_\nu\cdot\mathbf{b}\,\mathrm{d}(\delta\Sigma)\,. \tag{4.16}$$

For the variations resulting from the change of the size and shape of the dislocation only, the variation $\delta\Pi^0 = 0$, and (4.15) reduces to

$$\delta\Pi = \delta\tilde{U}_{\mathrm{c}} + \delta\tilde{U}_{\infty-\mathrm{c}} + \int_{\delta\Sigma} (\mathbf{t}^0_\nu + \hat{\mathbf{t}}_\nu)\cdot\mathbf{b}\,\mathrm{d}(\delta\Sigma)\,. \tag{4.17}$$

The evaluation of the variation $\delta\tilde{U}_{\infty-\mathrm{c}}$ has been the subject of a comprehensive study by Gavazza and Barnett [22]. This, as well as the evaluation of the core energy variation $\delta\tilde{U}_{\mathrm{c}}$, is beyond the scope of the present paper, which is concerned with the evaluation of the dislocation force only due to stress $\boldsymbol{\sigma}^0$ caused by externally applied loading and the image stress $\hat{\boldsymbol{\sigma}}$ of the dislocation.

In the expression (3.3) of Section 3, we used for δW the variation of the potential energy $\delta\Pi$ which includes the last term on the right-hand side of (4.17) only, i.e.,

$$\delta\Pi = \int_{\delta\Sigma} (\mathbf{t}^0_\nu + \hat{\mathbf{t}}_\nu)\cdot\mathbf{b}\,\mathrm{d}(\delta\Sigma)\,, \tag{4.18}$$

with the image traction $\hat{\mathbf{t}}_\nu$ omitted, because the dislocation force from the stress caused by external loading was only

considered there. It is also noted that (4.18) is an exact expression for $\delta\Pi$ if the virtual change of the dislocation configuration is restricted to be a rigid-body translation (or rotation, in the case of isotropic elastic medium), since then $\delta\tilde{U}_{\infty-c} = 0$ and $\delta\tilde{U}_c = 0$ identically.

By substituting $\mathbf{t}_\nu^0 = \boldsymbol{\sigma}^0 \cdot \boldsymbol{\nu}$ and $\hat{\mathbf{t}}_\nu = \hat{\boldsymbol{\sigma}} \cdot \boldsymbol{\nu}$ into (4.18), we obtain

$$\delta\Pi = \int_{\delta\Sigma} [(\boldsymbol{\sigma}^0 + \hat{\boldsymbol{\sigma}}) \cdot \mathbf{b}]\, \mathrm{d}(\delta\boldsymbol{\Sigma}), \quad \mathrm{d}(\delta\boldsymbol{\Sigma}) = \boldsymbol{\nu}\mathrm{d}(\delta\Sigma), \tag{4.19}$$

which is the representation of $\delta\Pi$ used for the derivation of the Peach–Koehler force in the next section.

4.2. *Peach–Koehler force*

As in Section 3, suppose that the dislocation loop evolves from its configuration C to a nearby configuration $C + \delta C$ by small displacements $\delta\mathbf{r}$ specified along C (Fig. 5b). The vectorial surface element of $\delta\Sigma$ is $\mathrm{d}(\delta\boldsymbol{\Sigma}) = \delta\mathbf{r} \times (\boldsymbol{\xi}\, \mathrm{d}l)$, where $\boldsymbol{\xi}$ is the unit vector along the dislocation line, and dl is the length element of this line. The substitution of this expression in (4.19) gives

$$\delta\Pi = \oint_C \delta\mathbf{r} \cdot \{\boldsymbol{\xi} \times [(\boldsymbol{\sigma}^0 + \hat{\boldsymbol{\sigma}}) \cdot \mathbf{b}]\}\, \mathrm{d}l. \tag{4.20}$$

The configurational force (per unit length of the dislocation) $\mathbf{f}$ is defined by the requirement that the line integral of its work on the displacement $\delta\mathbf{r}$ along the dislocation loop is equal to $-\delta\Pi$, i.e.,

$$\oint_C (\mathbf{f} \cdot \delta\mathbf{r})\, \mathrm{d}l = -\delta\Pi. \tag{4.21}$$

The negative sign in front of $\delta\Pi$ in (4.21) is used, because if the dislocation loop spontaneously moves from its configuration C to $C + \delta C$, the potential energy must decrease ($\delta\Pi < 0$); the released energy provides a driving force for the dislocation movement. The comparison of (4.20) and (4.21) establishes the Peach–Koehler type expression for the dislocation force

$$\mathbf{f} = [(\boldsymbol{\sigma}^0 + \hat{\boldsymbol{\sigma}}) \cdot \mathbf{b}] \times \boldsymbol{\xi}. \tag{4.22}$$

By a different route, this expression, involving the image stress of the dislocation, was first derived by Gavazza and Barnett [35]. Its particular case, applicable to glide dislocations with the slip discontinuity, was derived and used to study the equilibrium configurations of large number of dislocations by Lubarda [39], Van der Giessen and Needleman [40], Deshpande et al. [41], and others. If there are more than one dislocation in the body, and if interactions among them are included in the analysis, the expression (4.22) becomes

$$\mathbf{f} = [(\boldsymbol{\sigma}^0 + \hat{\boldsymbol{\sigma}} + \boldsymbol{\sigma}^{\mathrm{int}}) \cdot \mathbf{b}] \times \boldsymbol{\xi}, \tag{4.23}$$

where $\boldsymbol{\sigma}^{\mathrm{int}}$ is the interaction stress caused by all other dislocations at the considered point of the dislocation loop, while $\hat{\boldsymbol{\sigma}}$ represents the sum of the image stress fields from all dislocations. See also the energy based derivation of the Peach-Koehler force presented by Le [34].

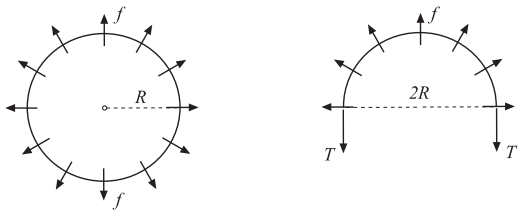

Fig. 15 – (a) A circular dislocation loop of radius R under uniformly distributed glide force *f*. (b) A free-body diagram of one-half of the loop. The dislocation line tension *T* balances the distributed dislocation force *f*.

4.3. *Self-force due to dislocation itself*

The self-stress field is singular at the points along the dislocation loop. Gavazza and Barnett [22] showed that the self-force on a loop element (the dislocation force due to the dislocation loop itself) depends on the local curvature of the loop, on certain elastic data for an infinite straight dislocation tangent to the loop, and on the cut-off radius ρ, used to define a tabular region along the loop within which the elastic fields are not well-described by the linear elasticity. This cut-off radius was assumed to be constant along the loop, but unspecified by the analysis. Nonlinear elasticity or atomistic simulations within the tube are needed to better address the problem of the determination of the dislocation loop self-force [42–45]. For a dislocation in an anisotropic crystal, the segment may also experience a force which acts to rotate it toward the orientation of a lower energy in the lattice [46]. In silicon, which has a diamond cubic structure, there are three low-energy orientations of the dislocation line relative to the Burgers vector and the loop tends to take a hexagonal shape [47,48]. In dynamic problems of a nonuniformly moving dislocation, there may be a contribution to self-force, even for a straight dislocation, from the stress waves emitted by dislocation during its entire history of motion [14,24,49–54].

4.4. *Dislocation line tension*

The presence of a dislocation loop in an elastic body gives rise to strain energy stored in the body. One may expect that the stored energy is smaller for smaller (shorter) loops. To decrease its strain energy, a spontaneous tendency of the material is to shrink a dislocation loop (decrease its length) and possibly get rid of it altogether [12]. Consequently, one may consider that dislocation loop is under a line tension which opposes its expansion, similarly to a taut string. This line tension is approximately equal to the self-strain energy of a dislocation loop per unit its length. To show that this is so, consider a circular dislocation loop of radius R under uniform Peach-Koehler glide force f, orthogonal to the loop at each of its points (Fig. 15a). Denote the strain energy per unit length of dislocation by E_o, and assume that E_o is independent of R. Suppose that the dislocation experiences a virtual expansion, so that its radius increases by δR. The corresponding work done by f must be equal to the increase of the strain

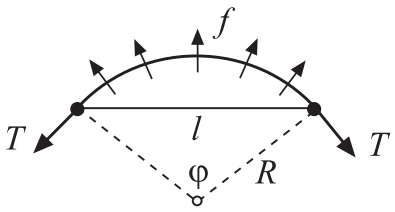

Fig. 16 – An infinitesimal bow-out of a pinned segment of a dislocation line whose initial length is l. Under an applied stress giving rise to a dislocation force *f*, the radius of curvature is R and the angle spanned by a circular cord is φ, such that $l = 2R\sin(\varphi/2)$. The dislocation line tension is *T*.

energy caused by the increase of the length of the dislocation, i.e., $2\pi R f\delta R = E_o 2\pi\delta R$. This gives

$$E_o = fR\,. \tag{4.24}$$

On the other hand, the equilibrium consideration of a half of the loop (Fig. 15b) requires that the dislocation line tension ($2T$) carries the sum of the vertical components of f over the length of a semi-circular loop ($2T = f\cdot 2R$), which gives

$$T = fR\,. \tag{4.25}$$

By comparing (4.24) and (4.25), it follows that the line tension is indeed equal to the dislocation strain energy per unit of its length,

$$T = E_o\,. \tag{4.26}$$

If the interactions of different segments of dislocation loop are ignored, the energy E_o may be taken as the specific strain energy of an infinitely long straight dislocation tangent to the dislocation loop at the considered point of the loop (e.g., [9, p. 263]).

An instructive alternative derivation of the line tension expression is based on the consideration of an infinitesimal bow-out of a pinned segment of dislocation under an applied stress, which gives rise to dislocation force f along that segment (Fig. 16). The equilibrium condition for the bowed-out dislocation segment gives $T = fR$. The work done by f in bowing-out the dislocation segment from its straight configuration of length l to a circular arc of length $R\varphi$ is $(1/2)fA$, where $A = (1/2)R^2(\varphi - \sin\varphi)$ is the area of a swept circular segment. This must be equal to the change of the strain energy $(R\varphi - l)E_o$, where $l = 2R\sin(\varphi/2)$. In the limit of small φ, this analysis reproduces the expression (4.24) and thus (4.26). The greater the line tension T, the greater the radius $R = T/f$, i.e., the harder (more energy-demanding) to bow-out the dislocation. Further analysis of the dislocation line tension, including its dependence on the radius of curvature of dislocation and its orientation, can be found in Cai and Nix [9], and Anderson et al. [10].

5. Determination of the dislocation force from the J-integral

The Peach–Koehler expression for the configurational force on a dislocation can also be derived by using the formalism of the configurational mechanics [29,30,55–57], specifically by evaluating the so-called J-integral around the dislocation. There have been numerous contributions to the study of configurational forces on material defects, such as cracks, dislocations, voids, inclusions, and grain or phase boundaries; a comprehensive survey of the field can be found in the review papers or books by Maugin [58], Gurtin [59], and Kienzler and Herrmann [60].

We restrict the consideration in this section to an edge dislocation embedded in an elastic isotropic body of arbitrary shape under the conditions of plane strain (Fig. 15). Similar analysis can be performed in the case of a screw dislocation or a mixed edge-screw dislocation. For simplicity, we assume that the boundary of the body is traction-free; thus, we evaluate the dislocation force arising from the image stress only (i.e., from the attraction exerted on the dislocation by the free boundary of the body). An analogous derivation proceeds with the included external loading, or the interaction stresses caused by the presence of other dislocations. The J integrals of the plane strain infinitesimal elastic deformations are

$$J_\beta = \oint P_{\alpha\beta} n_\alpha \,\mathrm{d}l\,, \quad (\alpha,\beta) = 1,2\,, \tag{5.1}$$

evaluated over a closed contour whose infinitesimal element $\mathrm{d}l$ has the outward normal n_α. We use in this section the index notation with respect to the coordinate system (x_1, x_2), with the summation convention implied over the repeated index. The components of the energy momentum tensor $P_{\alpha\beta}$ [30] are

$$P_{\alpha\beta} = w\delta_{\alpha\beta} - \sigma_{\alpha\gamma}u_{\gamma,\beta}\,, \quad w = \frac{1}{2}\sigma_{\alpha\beta}\epsilon_{\alpha\beta}\,. \tag{5.2}$$

The strain energy density is denoted by w, $\delta_{\alpha\beta}$ are the components of the Kronecker delta tensor, and the comma specifies the indicated partial derivative. The in-plane strain components are related to the stress components by Hooke's law

$$\epsilon_{\alpha\beta} = \frac{1}{2G}\left(\sigma_{\alpha\beta} - \nu\sigma_{\gamma\gamma}\delta_{\alpha\beta}\right), \tag{5.3}$$

where G is the elastic shear modulus, ν is the Poisson ratio, and $\sigma_{\gamma\gamma} = \sigma_{11} + \sigma_{22}$.

Consider an edge dislocation parallel to the x_3 direction, having the Burgers vector $\mathbf{b} = \{b_1, b_2\}$ and residing in a finite body at some distance from its free boundary S (Fig. 17). The total elastic stress, strain, and displacement fields in the body are the sums of the elastic fields for a dislocation in an infinite medium and the image fields (Section 5), such that

$$\sigma_{\alpha\beta} = \tilde{\sigma}_{\alpha\beta} + \hat{\sigma}_{\alpha\beta}\,, \quad \epsilon_{\alpha\beta} = \tilde{\epsilon}_{\alpha\beta} + \hat{\epsilon}_{\alpha\beta}\,, \quad u_{\alpha,\beta} = \tilde{u}_{\alpha,\beta} + \hat{u}_{\alpha,\beta}\,. \tag{5.4}$$

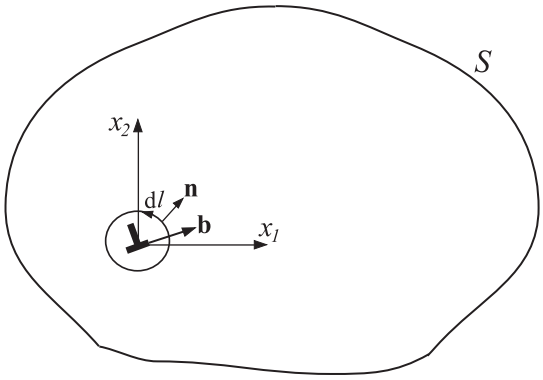

Fig. 17 – An edge dislocation with the Burgers vector b inside a finite body with the traction-free boundary S. Indicated is a small circle around the dislocation used to evaluate the *J*-integral. The line element of a circle is dl and its unit normal vector is n.

Upon the substitution of (5.4) into (5.2), the strain energy density can be expressed as

$$w = \tilde{w} + \hat{w} + w^{\text{int}}, \quad w^{\text{int}} = \tilde{\sigma}_{\alpha\beta}\hat{\epsilon}_{\alpha\beta}, \tag{5.5}$$

where

$$\tilde{w} = \frac{1}{2}\tilde{\sigma}_{\alpha\beta}\tilde{\epsilon}_{\alpha\beta}, \quad \hat{w} = \frac{1}{2}\hat{\sigma}_{\alpha\beta}\hat{\epsilon}_{\alpha\beta} \tag{5.6}$$

are the strain energy densities associated with the dislocation infinite medium and the image fields, respectively. The remaining term on the right-hand side of (5.5) is the interaction strain energy density w^{int}. Accordingly, from (5.2), the energy momentum tensor can be decomposed as

$$P_{\alpha\beta} = \tilde{P}_{\alpha\beta} + \hat{P}_{\alpha\beta} + P^{\text{int}}_{\alpha\beta}, \tag{5.7}$$

in which

$$\tilde{P}_{\alpha\beta} = \tilde{w}\delta_{\alpha\beta} - \tilde{\sigma}_{\alpha\gamma}\tilde{u}_{\gamma,\beta}, \quad \hat{P}_{\alpha\beta} = \hat{w}\delta_{\alpha\beta} - \hat{\sigma}_{\alpha\gamma}\hat{u}_{\gamma,\beta} \tag{5.8}$$

are the energy momentum tensors associated with the dislocation infinite medium fields and the image fields, separately. The remaining part of the energy momentum tensor in (5.7) is the interaction part (see, also, [61])

$$P^{\text{int}}_{\alpha\beta} = w^{\text{int}} - (\tilde{\sigma}_{\alpha\gamma}\hat{u}_{\gamma,\beta} + \hat{\sigma}_{\alpha\gamma}\tilde{u}_{\gamma,\beta}). \tag{5.9}$$

In view of the Hooke's law (5.3), $w^{\text{int}} = \tilde{\sigma}_{\alpha\beta}\hat{\epsilon}_{\alpha\beta}$ can be expressed solely in terms of stresses, so that (5.9) becomes

$$P^{\text{int}}_{\alpha\beta} = \frac{1}{2G}\left(\tilde{\sigma}_{mn}\hat{\sigma}_{mn} - \nu\tilde{\sigma}_{mm}\hat{\sigma}_{nn}\right)\delta_{\alpha\beta} - (\tilde{\sigma}_{\alpha\gamma}\hat{u}_{\gamma,\beta} + \hat{\sigma}_{\alpha\gamma}\tilde{u}_{\gamma,\beta}). \tag{5.10}$$

Upon the substitution of (5.7) into (5.1), the J_β integrals can be additively decomposed as

$$J_\beta = \tilde{J}_\beta + \hat{J}_\beta + J^{\text{int}}_\beta, \tag{5.11}$$

where

$$\tilde{J}_\beta = \oint \tilde{P}_{\alpha\beta}n_\alpha \,\mathrm{dl}, \quad \hat{J}_\beta = \oint \hat{P}_{\alpha\beta}n_\alpha \,\mathrm{dl}, \quad J^{\text{int}}_\beta = \oint P^{\text{int}}_{\alpha\beta}n_\alpha \,\mathrm{dl}. \tag{5.12}$$

To determine the configurational forces on the dislocation, the J_β integrals are evaluated around a small circle of radius r about the center of the dislocation (Fig. 15). The $\tilde{J}_\beta$ integrals in (5.12) vanish because the dislocation alone in an infinite medium does not exert any force on itself. The $\hat{J}_\beta$ integrals also vanish, because the image elastic field is non-singular within a circle around the dislocation. Thus, (5.11) reduces to

$$J_\beta = J^{\text{int}}_\beta = \oint P^{\text{int}}_{\alpha\beta}n_\alpha \,\mathrm{dl}. \tag{5.13}$$

Its two components are

$$J_1 = \int_0^{2\pi} (P^{\text{int}}_{11}\cos\theta + P^{\text{int}}_{21}\sin\theta)r\,\mathrm{d}\theta,$$
$$J_2 = \int_0^{2\pi} (P^{\text{int}}_{12}\cos\theta + P^{\text{int}}_{22}\sin\theta)r\,\mathrm{d}\theta, \tag{5.14}$$

which represent the x_1 and x_2 component of the dislocation force exerted on the dislocation by the image field. This is so because the J_β integrals represent the energy release rates associated with the translation of the defect in the x_β direction [56,57].

5.1. *Peach–Koehler force*

We use (5.14) to derive the expression for the Peach–Koehler force on the dislocation. The well-known stress and displacement fields for the edge dislocation in an infinite medium are listed in Appendix A of the paper. Although the determination of the image fields would require numerical procedure, e.g., the use of the finite-element method, we can proceed with the analysis without this evaluation by observing that along a sufficiently small circle around the dislocation, the image stresses and the displacement gradients are nearly uniform, so that they can be taken out of the integrals in (5.14). Upon performing the integration, we obtain for an edge dislocation with the Burgers vector b_1,

$$\begin{aligned}\int_0^{2\pi} P^{\text{int}}_{11}\cos\theta\, r\,\mathrm{d}\theta &= \frac{b_1}{8(1-\nu)}\left[\hat{\sigma}_{12}(5-4\nu) - 2G\hat{u}_{2,1}\right],\\ \int_0^{2\pi} P^{\text{int}}_{21}\sin\theta\, r\,\mathrm{d}\theta &= \frac{b_1}{8(1-\nu)}\left[\hat{\sigma}_{12}(3-4\nu) + 2G\hat{u}_{2,1}\right].\end{aligned} \tag{5.15}$$

The substitution of (5.15) into (5.14) then yields $J_1 = \hat{\sigma}_{12}b_1$, which is the Peach–Koehler expression for the horizontal component of the force exerted on the dislocation by the image stress from the free boundary of the body. The vertical component is $J_2 = -\hat{\sigma}_{11}b_1$. If the b_2 component of the Burgers vector is included, the expressions for the J_1 and J_2 integrals are

$$J_1 = \hat{\sigma}_{21}b_1 + \hat{\sigma}_{22}b_2, \quad J_2 = -(\hat{\sigma}_{11}b_1 + \hat{\sigma}_{12}b_2). \tag{5.16}$$

For an alternative derivation, see Anderson et al. [10, pp. 86–88].

Evidently, the derivation of the Peach–Koehler expression for the dislocation force by the evaluation of *J*-integrals is more laborious than the derivation based on the direct consideration of the potential energy, used in Section 4. However, in specific problems the evaluation of *J*-integrals proceeds without direct evaluation of the stress components appearing in the Peach–Koehler force expression, which can significantly simplify the analysis [62–66]. For dynamic problems of moving dislocations, a four-dimensional (space/time) dynamic energy momentum tensor can be introduced and the dislocation force can be calculated from the dynamic *J* integral [67,68,52,69].

6. Conclusions

We reviewed in this paper different definitions of the Burgers vector used in the literature and the corresponding construction of the Burgers circuit for the dislocation loops and straight dislocations, created by the displacement discontinuity imposed across different surface cuts. This is used as a geometric background to derive the Peach–Koehler expression for the energetic force on a dislocation loop. Three approaches were adopted and compared: (i) the classical virtual work approach of Peach and Koehler, extended to include the changes in size and shape of the dislocation loop; (ii) the potential energy approach, which allows the incorporation of the effects of image stresses from the loaded, free, or constrained boundary; and (iii) the approach based on the evaluation of the *J*-integral. The magnitudes and directions of the glide and climb components of the dislocation force are determined and discussed for continuum and lattice different dislocations. The dislocation line tension and the osmotic force on a lattice dislocation are also briefly reviewed. Apart from being of research interest, the presented analysis may be appealing from the methodological point of view in a more comprehensive coverage of the topics of dislocations and configurational forces in graduate courses of solid mechanics and materials science.

Conflicts of interest

The author declares no conflicts of interest.

Acknowledgments

Research support from the Montenegrin Academy of Sciences and Arts is gratefully acknowledged. I thank Professor Marc A. Meyers for valuable discussions and for reading the manuscript and making helpful comments and suggestions.

REFERENCES

[1] Orowan E. Zur Kristallplastizität. III. Über den Mechanismus des Gleituorganges. Z Phys 1934;89:634–59.
[2] Polanyi M. Über eine Art Gitterstorung, die einen Kristall Plastisch Machen Kinnte. Z Phys 1934;80:660–4.
[3] Taylor GI. The mechanism of plastic deformation of crystals. Part I: Theoretical. Proc R Soc Lond Sect A 1934;145:362–87.
[4] Volterra V. Sur l'équilibre des corps élastiques multiplement convexes. Ann Ec Norm Ser 3 1907;24:401–517.
[5] Peach M, Koehler JS. The forces exerted on dislocations and the stress fields produced by them. Phys Rev 1950;80(3):436–9.
[6] Kröner E. Kontinuumstheorie der Versetzungen und Eigenspannungen. Berlin: Springer-Verlag; 1958.
[7] Friedel J. Dislocations. Oxford: Pergamon Press; 1964.
[8] Hirth JP, Lothe J. Theory of dislocations. 2nd ed. New York: John Wiley & Sons; 1982.
[9] Cai W, Nix WD. Imperfections in crystalline solids. Cambridge: Cambridge Univ. Press; 2016.
[10] Anderson PM, Hirth JP, Lothe J. Theory of dislocations. 3rd ed. New York: Cambridge Univ. Press; 2017.
[11] Seeger A. Theorie der Gitterfehlstellen. In: Flügge S, editor. Handbuch der Physik. Berlin: Springer; 1955. p. 383–665. Vol. VII-1 (Crystal Physics I).
[12] Weertman J, Weertman JR. Elementary dislocation theory. New York: Macmillan; 1964.
[13] de Wit R. The direction of the force on a dislocation and the sign of the Burgers vector. Acta Met 1965;13:1210–1.
[14] Eshelby JD. Aspects of the theory of dislocations. In: Hopkins HG, Sewell MJ, editors. Mechanics of solids: the rodney hill 60th anniversary volume. Oxford: Pergamon Press; 1982. p. 185–225.
[15] Balluffi RW. Introduction to elasticity theory for crystal defects. 2nd ed. New Jersey: World Scientific; 2016.
[16] Ashby MF, Jones DRH. Engineering materials, vol. 1. 2nd ed. Oxford: BH; 2000.
[17] Teodosiu C. Elastic models of crystal defects. Berlin: Springer-Verlag; 1982.
[18] Hertzberg RW. Deformation and fracture mechanics of engineering materials. 4th ed. New York: John Wiley & Sons; 1996.
[19] Smith W, Hashemi J. Foundations of materials science and engineering. New York: McGraw-Hill; 2010.
[20] Askeland DR, Phulé PP. Essentials of materials science and engineering. Victoria: Thomson; 2004.
[21] Hull D, Bacon DJ. Introduction to dislocations. 4th ed. Oxford: Butterworth Heinemann; 2001.
[22] Gavazza SD, Barnett DM. The self-force on a planar dislocation loop in an anisotropic linear-elastic medium. J Mech Phys Solids 1976;24:171–85 (with Errata, JMPS 24, p. 397).
[23] Asaro RJ, Lubarda VA. Mechanics of solids and materials. Cambridge: Cambridge Univ. Press; 2006.
[24] Nabarro FRN. Theory of crystal dislocations. New York: Dover Publications; 1967.
[25] Lubarda VA. Dislocation equilibrium conditions revisited. Int J Solids Struct 2006;43:3444–58.
[26] Peierls R. The size of a dislocation. Proc Phys Soc 1940;52:37–40.
[27] Nabarro FRN. Dislocations in a simple cubic lattice. Proc Phys Soc 1947;59:256–72.
[28] Kelly A, Knowles KM. Crystallography and crystal defects. 2nd ed. New York: John Wiley & Sons; 2012.
[29] Eshelby JD. The force on an elastic singularity. Philos Trans R Soc A 1951;244:87–112.
[30] Eshelby JD. The continuum theory of lattice defects. Solid State Phys 1956;3:79–144.
[31] Tadmor EB, Ortiz M, Phillips R. Quasicontinuum analysis of defects in solids. Philos Mag A 1996;73:1529–63.
[32] Phillips R. Crystals, defects and microstructures: modeling across scales. Cambridge: Cambridge Univ. Press; 2001.
[33] Mura T. Micromechanics of defects in solids. 2nd rev. ed Dordrecht, The Netherlands: Kluwer Academic Publishers; 1987.

[34] Le KC. Introduction to micromechanics. New York: Nova Science Publ., Inc.; 2010.
[35] Gavazza SD, Barnett DM. The image force on a dislocation loop in a bounded medium. Scripta Metall 1975;9:1263–5.
[36] Lubarda VA, Blume JA, Needleman A. An analysis of equilibrium dislocation distributions. Acta Metall Mater 1993;41:625–42.
[37] Bower AF. Applied mechanics of solids. Boca Raton, FL: CRC Press, Taylor & Francis Group; 2010.
[38] Lubarda VA. Energy analysis of dislocation arrays near bimaterial interfaces. Int J Solids Struct 1997;34:1053–73.
[39] Lubarda VA. On the elastic strain energy representation of a dislocated body and dislocation equilibrium conditions. J Elasticity 1993;32:19–35.
[40] Van der Giessen E, Needleman A. Discrete dislocation plasticity: a simple planar model. Model Simul Mater Sci Eng 1995;3:689–735.
[41] Deshpande VS, Needleman A, Van der Giessen E. Finite strain discrete dislocation plasticity. J Mech Phys Solids 2003;51:2057–83.
[42] Bulatov VV, Cai W. Computer simulations of dislocations. Oxford: Oxford Univ. Press; 2006.
[43] Cai W, Arsenlis A, Weinberger CR, Bulatov VV. A non-singular continuum theory of dislocations. J Mech Phys Solids 2006;54:561–87.
[44] Yin J, Barnett DM, Cai W. Efficient computation of forces on dislocation segments in anisotropic elasticity. Model Simul Mater Sci Eng 2010;18:045013.
[45] Szajewski BA, Pavia F, Curtin WA. Robust atomistic calculation of dislocation line tension. Model Simul Mater Sci Eng 2015;23:085008.
[46] Fitzgerald SP, Aubry S. Self-force on dislocation segments in anisotropic crystal. J Phys Condens Matter 2010;22:295403.
[47] Dash WC. Dislocations and mechanical properties of crystals. New York: John Wiley; 1957.
[48] Liu GCT, Li JCM. Energy of hexagonal dislocation loops. Phys Stat Sol 1966;18:527–39.
[49] Kosevich AM. Crystal dislocations and the theory of elasticity. In: Nabarro FRN, editor. Dislocations in solids, vol. 1. Amsterdam: North-Holland; 1979. p. 33–141.
[50] Weertman J, Weertman JR. Moving dislocations. In: Nabarro FRN, editor. Dislocations in solids, vol. 3. North-Holland, Amsterdam; 1980. p. 19–59.
[51] Markenscoff X. The transient motion of a nonuniformly moving dislocation. J Elast 1980;10:19–201.
[52] Ni L, Markenscoff X. The self-force and effective mass of a generally accelerating dislocation. I: Screw dislocation. J Mech Phys Solids 2008;56:1348–79.
[53] Meyers MA, Jarmakani H, Bringa E, Remington BA. Dislocations in shock compression and release. In: Hirth J, Kubin L, editors. Dislocations in solids, vol. 15. Elsevier; 2009. p. 91–197.
[54] Meyers MA, Traiviratana S, Lubarda VA, Benson DJ, Bringa EM. The role of dislocations in the growth of nanosized voids in ductile failure of metals. J Mater 2009;61:35–41.
[55] Rice JR. A path independent integral and approximate analysis of strain concentration by notches and cracks. J Appl Mech 1968;38:379–86.
[56] Knowles JK, Sternberg E. On a class of conservation laws in linearized and finite elastostatics. Arch Ration Mech Anal 1972;44:187–211.
[57] Budiansky B, Rice JR. Conservation laws and energy-release rates. J Appl Mech 1973;40:201–3.
[58] Maugin GA. Configurational forces: thermomechanics, physics, mathematics and numerics. Boca Raton, Florida: CRC Press/Taylor & Francis; 2011.
[59] Gurtin ME. Configurational forces as basic concepts of continuum mechanics. New York: Springer-Verlag; 2000.
[60] Kienzler R, Herrmann G. Mechanics in material space. Berlin: Springer; 2001.
[61] Lubarda VA. On the determination of interaction forces between parallel dislocations by the J integral evaluation. Cont Mech Thermodyn 2016;28:391–405.
[62] Eshelby JD. The calculation of energy release rates. In: Sih GC, editor. Prospects of fracture mechanics. Leyden, The Netherlands: Noordhof; 1975. p. 69–84.
[63] Freund LB. Stress intensity factor calculations based on a conservation integral. Int J Solids Struct 1978;14: 241–50.
[64] Rice JR. Conserved integrals and energrtic forces. In: Bilby BA, Miller KJ, Willis JR, editors. Fundamentals of deformation and fracture (Eshelby Memorial Symposium). Cambridge University Press; 1985. p. 33–56.
[65] Lubarda VA, Markenscoff X. Dual conservation integrals and energy release rates. Int J Solids Struct 2007;44: 4079–91.
[66] Lubarda VA. The energy momentum tensor in the presence of body forces and the Peach–Koehler force on a dislocation. Int J Solids Struct 2008;45:1536–45.
[67] Eshelby JD. Energy relations and the energy-momentum tensor in continuum mechanics. In: Kanninen MF, Adler WF, Rosenfield AR, Jaffee RI, editors. Inelastic behaviour of solids. New York: McGraw-Hill; 1970. p. 77–115.
[68] Fletcher DC. Conservation laws in linear elastodynamics. Arch Ration Mech Anal 1976;60:329–53.
[69] Markenscoff X, Huang S. The energetics of dislocations accelerating and decelerating through the shear-wave speed barrier. Appl Phys Lett 2009;94:021906.
[70] Meyers MA, Chawla KK. Mechanical behavior of materials. 2nd ed. Cambridge: Cambridge Univ. Press; 2008.